Vegetation greening intensified soil drying in some semi-arid and arid areas of the world

Yuanhong Deng[a,b], Shijie Wang[a,c], Xiaoyong Bai[a,d,e,*], Guangjie Luo[e], Luhua Wu[a,b], Fei Chen[a,f], Jinfeng Wang[a,f], Chaojun Li[a,g], Yujie Yang[a,g], Zeyin Hu[a,b], Shiqi Tian[a,g], Qian Lu[a,f]

[a] State Key Laboratory of Environmental Geochemistry, Institute of Geochemistry, Chinese Academy of Sciences, Guiyang 550081, China
[b] University of Chinese Academy of Sciences, Beijing 100049, China
[c] Puding Karst Ecosystem Observation and Research Station, Chinese Academy of Sciences, Puding 562100, China
[d] CAS Center for Excellence in Quaternary Science and Global Change, Xi'an, 710061, China
[e] Guizhou Provincial Key Laboratory of Geographic State Monitoring of Watershed, Guizhou Education University, Guiyang 550018, China
[f] College of resources and environmental engineering, Guizhou University, Guiyang 550025, China
[g] School of Geography and Environmental Sciences, Guizhou Normal University, Guiyang 550001, China

ARTICLE INFO

ABSTRACT

Vegetation greening and soil drying, which are simultaneously observed, have brought controversy about whether vegetation greening leads to soil drying or wetting. Relevant conclusions from previous small-scale research are uncertain worldwide, and the indirect effects of climate via vegetation change on soil moisture (SM) are poorly understood. Here, to explore the effects of vegetation greening on SM change, the patterns of SM trends (wetting to more wetting (W to W), wetting to drying (W to D), drying to wetting (D to W) and drying to more drying (D to D)) were identified in the global vegetation greening (GVG) areas from 1982 to 2015 by using the turning years in the quantity of vegetation greenness and then validated by structural equation model (SEM) and 400 ground stations. The main results are as follows: 1) In the study period, 65.87% (33.57%, Sig.) of the GVG areas featured soil drying including the southeast of the United States, Africa north of the equator, the inland of Europe, the south of China and the inland of Australia, which were mainly from grasslands, barren, savannas, open shrublands, woody savannas and croplands. 2) Vegetation significantly and negatively influenced the average SM of global greening and drying areas, and their climate was arider than that in global greening and wetting areas. 3) Soil in over half of the GVG areas was toward drying after vegetation greenness increased but only the D to D pattern was mainly distributed in drylands (Semi-arid, Arid and Hyper-arid areas) such as the Loess Plateau of China and eastern Australia. The W to W and W to D patterns were remarkably observed in the in-situ SM. 4) SEM showed that the direct effects of vegetation increase on W to W and D to D patterns were stronger than those of temperature and precipitation, especially that the indirect effect of temperature on D to D pattern via promoting vegetation greening outweighed the direct effect of temperature. Overall, the increase in vegetation mainly caused by climate warming has exacerbated the tendency of soil drying in some drylands. Therefore, vegetation restoration or forestry management requires the consideration of local SM-carrying capacity for plants, especially in Semi-arid and Arid ecosystems.

1. Introduction

Vegetation, as the most basic component of ecosystem, has valuable ecological services, such as carbon sequestration and oxygen release, water conservation and land degradation prevention (Chen et al., 2019; Tong et al., 2018); thus, its increase is usually considered a benign development of an ecosystem. Affected by atmospheric CO_2 fertilization, climate change and human disturbance (Brandt et al., 2017; Silva et al., 2016; Zhao et al., 2018; Zhu et al., 2016), many parts of the world, such as China, India, southeast Australia, and semi-arid areas represented by African Sahel, are turning green (Chen et al., 2019; Fensholt et al., 2012). However, sustainable vegetation growth requires

---

* Corresponding author.
  E-mail address: baixiaoyong@vip.skleg.cn (X. Bai).

sufficient water supply, and the pressure of water resources consumed by human production and living as well as ecological utilization has become gradually prominent (Liu et al., 2017). For example, at the end of the 21st century, over 42% of the global vegetated area was predicted to have the characteristic of simultaneous vegetation greening and soil drying in summer under a high representative concentration pathway (RCP 8.5) scenario (Mankin et al., 2018; Veldkamp et al., 2016); vegetation restoration in the Loess Plateau of China was reaching the threshold of soil water-carrying capacity of vegetation (Feng et al., 2016). Furthermore, vegetation influences the interception, infiltration, and evaporation in the water cycle (Stothoff et al., 1999; Sun et al., 2006), therefore it is imperative to reveal the hydrological effects of vegetation dynamic change, which is an important research issue of eco-hydrology (D'odorico et al., 2010). Soil moisture (SM) is an indispensable factor involved in hydrological processes, energy conversion, climate change, and ecological processes (Adair et al., 2011; Deng et al., 2019; Porporato et al., 2002; Stocker et al., 2019). Most importantly, Precipitation, surface runoff, and groundwater are usually converted into SM before they can be absorbed and utilized by vegetation, and SM is the key to the interaction of most land vegetation with hydrological processes and climate fluctuations (Rodriguez-Iturbe, 2000). Therefore, the variation of SM and its response to vegetation change are particularly essential in the fields of water resources and vegetation's eco-hydrological processes.

Currently, many scholars mainly focus on the influence of vegetation type or its shifts on spatial distribution and temporal change of SM in water-limited or semi-arid areas, leaving a conspicuous knowledge gap about the mechanism of vegetation affecting SM, especially under the circumstances of climate change. D'odorico et al. (2007) studied the control of vegetation composition and structure on SM and found that SM in vegetation patches was higher than that in bare land; Chen et al. (2007) compared the relationship between five vegetation types and soil dynamics to find the vegetation type suitable for limited water resources; Wang et al. (2015) used four-year observation data and found that in semi-arid sand dunes, vegetation growth reduced the temporal stability of SM. The above reflects the lack of research about the role of vegetation increase in SM change on a longer-term and larger scale. Meanwhile, scale effects exist in vegetation eco-hydrology (Li et al., 2017), and due to the diversity in climate and soil conditions, the influence of vegetation on hydrological processes presents great spatial heterogeneity (Li et al., 2018), and many existing findings from small scales such as plot scale and slope scale (Jost et al., 2012), especially those from vegetation restoration involving human activities, have promoted the study of vegetation ecohydrology but may not be universally applicable at regional or global scale. Moreover, relevant conclusions on whether vegetation greening causes soil drying or wetting remain controversial. Several studies have pointed out that vegetation greening increased evapotranspiration and resulted in excessive soil water consumption (Feng et al., 2016; Zeng et al., 2018), and severely, caused more ecological droughts (Tietjen et al., 2017); however, other studies have proposed that vegetation had the ecological function of water conservation and storage (Feng et al., 2018), and the growth of precipitation caused by increased vegetation can even compensate for SM loss resulted from the enhanced surface evapotranspiration (Li et al., 2018). Thus, the influential law and mechanism of vegetation greening on the trend of SM change (especially, the declining trend) across the globe must be explored, which is practically crucial for sustainable vegetation production and water resource problem alleviation.

Here, we select the global vegetation greening (GVG) areas from 1982 to 2015 as the research area and aim to 1) reveal where vegetation greening and soil drying occurred simultaneously, 2) verify where and how SM trend changed after the mean value of vegetation greenness significantly increased, 3) explore how vegetation greening affected SM change by applying the stepwise regression and structural equation model, and 4) discuss whether the findings from gridded data

can pass the validation of SM from observational stations.

2. Materials and methods

2.1. Materials

2.1.1. Normalized Difference Vegetation Index (NDVI)

NDVI, obtained through the spectral absorption and reflection of plants, is sensitive to the growth status and biochemical characteristics of land vegetation, and can well reflect the "greenness" information of land surface (Fensholt et al., 2012). In this study, the Global Inventory Monitoring and Modeling System (GIMMS) NDVI3g product from 1982 to 2015 was used as a proxy for vegetation growth with a 15-day interval and a spatial resolution of 8 km, and it is widely applied in the research of vegetation coverage change (de Jong et al., 2011; Yang et al., 2019) and ecological processes (Huang et al., 2018).

2.1.2. ERA-Interim SM

Given the uneven distribution and short observation time of SM from stations, this study selected SM data from the European Center for Medium-Range Weather Forecasts' Reanalysis (ERA)-Interim (https://www.ecmwf.int/) with a resolution of 0.125° on a monthly scale. The SM product was improved using an extended Kalman filter, which can flexibly integrate microwave data. Moreover, this dataset can well capture the spatiotemporal changes of SM from observational stations (Albergel et al., 2012; Deng et al., 2020a; Deng et al., 2020b). Albergel et al. (2012) validated the ERA-Interim SM in 2007–2010 by using in-situ observational SM data around the global land and found that they correlated well with the average correlation coefficient of 0.7. The product includes 0–7, 7–28, 28–100, 100–289 cm SM data. Given that the shallow SM can represent deep SM in some cases (Qiu et al., 2014), the 0–7 cm SM data in 1982–2015 from ERA-Interim were used in this study.

2.1.3. Climate data

Precipitation and climate data from the Climatic Research Unit (CRU) time-series data version 4.01 were provided by East Anglia University in Britain. Based on the integration of observed data from global meteorological stations and data from several well-known databases, the gridded data covered the global land with temporal and spatial resolutions of monthly and 0.5°, respectively. Presently, CRU reanalysis data are used as basic climate data in research about hydrological and climatic processes (Ali et al., 2015).

2.1.4. Auxiliary data

High-precision (30 arc-seconds) aridity index map covering the global land was obtained from the Consultative Group for International Agricultural Research-Consortium for Spatial Information (http://www.cgiar-csi.org). The Penman-Monteith reference evapotranspiration equation was used to demonstrate the water availability of potential growth of reference vegetation. Following United Nations Environment Program (UNEP)'s climate classification based on aridity index, the global climate was divided into five types (Fig. 1), namely, Hyper-arid (<0.03), Arid (0.03–0.2), Semi-arid (0.2–0.5), Dry sub-humid (0.5–0.65), and Humid (>0.65). In the study, humid climate includes Dry sub-humid and Humid, while the arid climate consists of Semi-arid, Arid, and Hyper-arid.

MODIS land cover type product version 6 (MCD12C1V006, https://doi.org/10.5067/MODIS/MCD12C1.006) showed the yearly distribution of 17 land cover types worldwide in 2001–2017 with its spatial resolution of 500 m (Friedl et al., 2002). Considering the research goals, the study utilized the land cover map in 2001 and removed the water bodies, permanent wetlands, permanent snow, and ice.

SM data from stations were freely obtained from the International
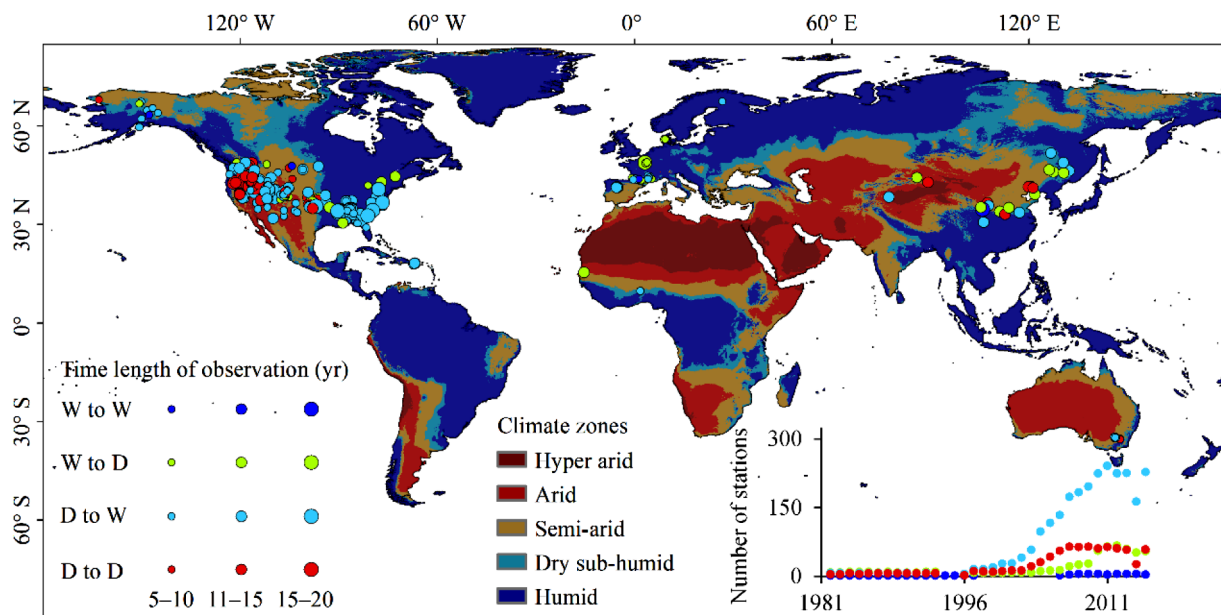
Fig. 1. Classification of global climate zones and spatial distribution and observation time length of SM stations for four SM trend patterns. The inserted scatter plot shows the number of effective stations of the four patterns in each year; meanwhile, colors of circle dots on the spatial map and colors of the inserted scatter plot represent four SM trend patterns, namely, blue, yellow-green, sky-blue and red colors represent W to W, W to D, D to W and D to D respectively.

Soil Moisture Network (ISMN) and the detailed description can be found in https://ismn.geo.tuwien.ac.at/en/ (Dorigo et al., 2011).

During preprocessing, NDVI, precipitation, temperature, aridity index, and land cover were interpolated by using the nearest neighbor method to match the spatial resolution of the SM product.

2.2. Methods

2.2.1. Classification of SM trend patterns

Theil-Sen estimation and Mann-Kendall (MK) test are not easily affected by abnormal values (Li et al., 2018). Thus, the methods were adopted for the calculation of linear slope and its significance test for NDVI, SM, precipitation, and air temperature at the pixel scale. In this study, the Theil-Sen slope with the absolute value of Z from the MK test greater than or equal to 1.96 was considered significant.

Moving t-test was used to identify the year in which the NDVI mean value increased abruptly with a significant level of 0.05 in GVG (i. e., Theil-Sen slope of NDVI is over zero) areas (Zhang et al., 2014). Given that more than one year could exceed the t-threshold, the year in which the mean NDVI difference was the largest was regarded as the turning year, and then it divided the time series of NDVI and SM into two periods: the period before the turning year (T_1) and the period after the turning year (T_2). The sliding step in moving t-test was 5 years, and thus T_1 and T_2 were not less than 5 years and exceeded the shortest period (3–4 years) of SM change (Deng et al., 2020b; Zhang et al., 2004), which to some extent reduced the error of SM trend caused by the short time length in some areas. According to Table 1, changes of

SM trends were divided into four patterns: wetting to more wetting (W to W), wetting to drying (W to D), drying to wetting (D to W), and drying to more drying (D to D). When at least one significant change trend was found in the T_1 and T_2, the change was considered significant.

2.2.2. Verification of four SM trend patterns

The four patterns of SM trend were validated by ground observational SM data from the ISMN. The selective conditions of stations were as follows: 1) observation time was between 1982 and 2015; 2) the recorded SM data was available for at least 7 months in a year, and observation length (continuous or discontinuous) was at least 5 years to reduce the impact of short and inconsistent observation lengths; 3) observation depth was within the top 7 cm of soil; 4) SM data were deleted when their quality flag was D (questionable/dubious-geophysical based). Finally, 400 stations were selected and their distributions were presented in Fig. 1. The observational SM of each station was processed to yearly data, and the nearest neighbor interpolation method was used to extract the NDVI of the corresponding SM stations. Ultimately, the time series of NDVI and SM for each pattern (W to W, W to D, D to W, and D to D) were calculated by averaging SM at all stations belonging to the pattern for each year. Data vacancies existed for several years after quality control and data preprocessing, especially in 1994 and 1995, and the SM and NDVI time series in 1982–2015 were divided into two periods based on the missing data: P1 (referred period) and P2 (assumed period, with the NDVI mean value increasing remarkably).

2.2.3. Structural equation model

Structural equation model (SEM), proposed by Karlg Jöreskog, a Swedish statistician and psychometrist, in the mid-1970s, is a kind of statistical method and verification technology that adopts linear equation system to express the relationship between observed variables and potential variables and between potential variables (Jöreskog, 1970), which has the advantages of path and factor analyses. Based on the conceptual model established by theoretical research and experience, SEM can reflect the direct, indirect, and comprehensive effects among variables. This method has been applied in ecology and climatology (Fauchald et al., 2017; Shi et al., 2016; Weterings et al., 2018).

Table 1
Division of SM trend patterns under different scenarios. K_1 and K_2 are the trends of SM change in T_1 and T_2, respectively.

Number	Combination scenario	Pattern
I	$K_1 > 0, K_2 > 0, K_2 - K_1 > 0$	Wetting to Wetting (W to W)
II	$K_1 > 0, K_2 > 0, K_2 - K_1 < 0$	Wetting to Drying (W to D)
III	$K_1 > 0, K_2 < 0, K_2 - K_1 < 0$	
IV	$K_1 < 0, K_2 > 0, K_2 - K_1 > 0$	Drying to Wetting (D to W)
V	$K_1 < 0, K_2 < 0, K_2 - K_1 > 0$	
VI	$K_1 < 0, K_2 < 0, K_2 - K_1 < 0$	Drying to Drying (D to D)
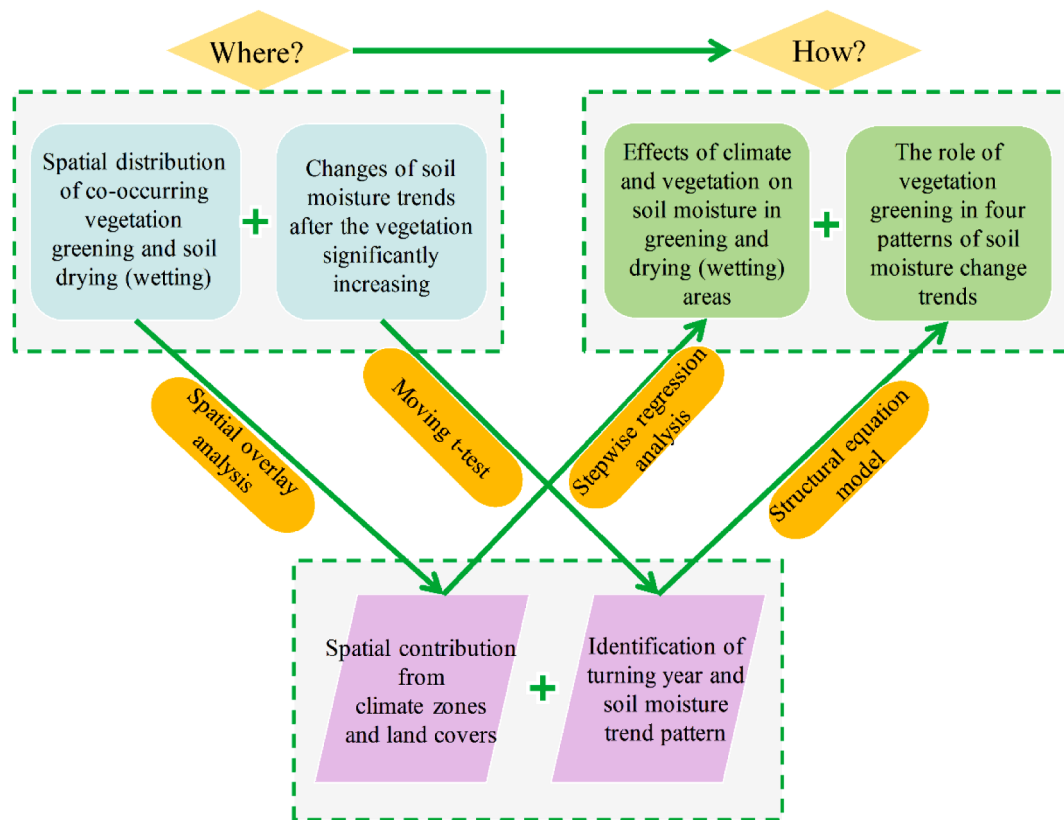
Fig. 2. Flow chart of this study

Interactions among NDVI, precipitation, temperature, and SM are complex. To reveal the impact of vegetation greening on the trend of SM change, the following hypotheses were designed: 1) the correlation between precipitation and temperature can weigh the climate condition of vegetation greening, i.e., the consistency of water and heat changes; 2) vegetation, precipitation, and temperature have direct effects on SM change; and 3) precipitation or temperature can play a direct role on vegetation and then produce indirect effects on SM via vegetation change (Tietjen et al., 2017). This research applied Amos software to construct and solve the SEM and used maximum likelihood method to estimate the path coefficients and parameters. In the study, SEM was saturated and thus the significance of the model could not be obtained (Lu et al., 2016).

Finally, the main objectives, contents, and methods of this study are shown in Fig. 2.

3. Results

3.1. Spatial distribution of coexisting greening and drying/wetting

The averaged greening rate of the GVG areas (0.94×10^{-3} yr^{-1}) was more than three times the averaged change rate of vegetation in global vegetation-covered areas (0.27×10^{-3} yr^{-1}). Spatially, 61.65% (38.46%, Sig.) of the global vegetated areas were greening and the contiguous areas with vegetation greening were overall consistent with previous research results (Fensholt et al., 2012), mainly located in India, Europe, the south of China and other areas; meanwhile, vegetation greenness in the Saharan Desert of Africa with Hyper-arid climate increased significantly, albeit slowly (Fig. 3). Furthermore, the surface SM in 65.87% (33.57%, Sig.) of the GVG area decreased mainly from Humid and Dry sub-humid areas, including the southeast of the United States, Brazilian Plateau, inland areas of Europe, Africa north of the equator, and the south of China, Semi-arid areas such as the middle of

North America and northern China, Arid areas including the inland of Australia, and Hyper-arid areas in Saharan of Africa. Under the background of global temperature rising (Fig. S1), areas where both vegetation and precipitation increased but soil dried in 1982–2015 accounted for 36.55% of GVG areas, including the northeastern United States, central Africa, Europe, and northwest Australia (Fig. S2).

3.2. Turning years and SM trend patterns

The turning years in which the average vegetation greenness increased abruptly differed in the GVG areas (Fig. 4a). Overall, the turning years of vegetation greenness in arid areas were late, such as the Sahara in Africa, inland region of eastern Australia, Northwest China, and the west of the United States. In humid areas, it was complex. For example, the turning year in southern Europe was earlier than that in northern Europe, while that in southeastern China was later than that in southeastern America at the same latitude. In Fig. S3, the distribution of increment in averaged NDVI after the turning year was basically in agreement with Fig. 3a. Fig. 4b demonstrates that after the average vegetation greenness increased abruptly in T_2, the SM trend in 55.77% (23.79%, Sig.) of the GVG areas was toward unfavorable directions (W to D and D to D). Concretely, the northwest coastal area of South America, the southern end of Africa, Europe and India belonged to the W to D pattern, i.e., the trend of soil wetting weakened or changed to the drying trend after the turning year, though the average SM in these areas increased variedly in Fig. S3b. The D to D pattern was mainly located in the Loess Plateau of China and eastern Australia where the trend of soil drying was enhanced after the turning year. According to previous studies (Feng et al., 2016; Yang et al., 2014), the Loess Plateau of China belonged to the D to D pattern, thus supporting the validity of the D to D pattern identified in the study. The W to W pattern had the smallest proportion, and its distribution was scattered. Additionally, SM trends in 37.19% (15.54%, Sig.) of the GVG areas,
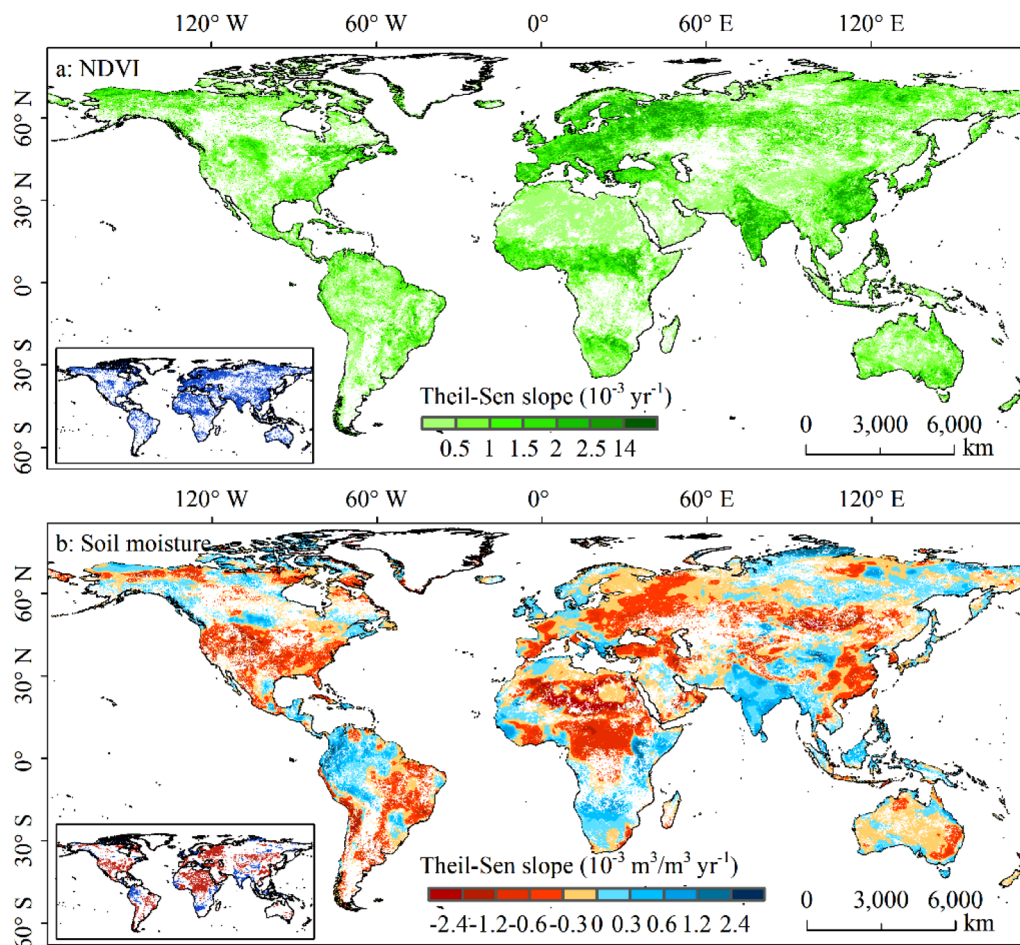
Fig. 3. Spatial distribution for Theil-Sen slopes of NDVI (a) and SM (b) in the GVG areas from 1982 to 2015. The inserted map in the lower left shows the spatial distribution for the significant Theil-Sen slopes (the absolute value of Z statistic from MK test ≥ 1.96) with the blue and red colors indicating the significant increase and decrease trends, respectively.

such as the southeastern United States, northern Mediterranean, and southern China, showed the D to W pattern, where the trend of soil drying weakened or changed to a wetting trend after vegetation greenness increased significantly. However, whether the above findings are attributed to the negative or positive effects of vegetation greening has yet to be verified.

3.3. Effects of vegetation and climate on SM change

3.3.1. Stepwise regression analysis at a regional scale

Land-atmosphere interaction is characterized by spatiotemporal dependence, and the regional average state can reflect the influence of a larger scale system state. In Fig. 5, the average annual precipitation, temperature, and vegetation increased significantly from 1982 to 2015 in the global soil drying and greening areas (D & G) as well as global soil wetting and greening areas (W & G). However, compared with W & G areas, the average annual precipitation in D & G areas was less with their difference of 133.62–272.42 mm. Stepwise multiple regression was used to reveal the effects of NDVI, precipitation, and temperature on SM, and its standardized regression coefficients can weigh the effect intensity of NDVI, precipitation, and temperature on SM (Oh and Ha, 2016). It demonstrated that the average SM in W & G areas was affected by the increase of vegetation and precipitation, while the average SM in D & G areas was influenced by the growth of vegetation and temperature. The coefficients indicated that vegetation exerted stronger effects on SM when compared with climatic factors, especially precipitation. Additionally, the explanatory power of vegetation,

precipitation, and temperature on SM change under the two scenarios exceeded 50%.

3.3.2. SEM results of four SM trend patterns

The area-averaged annual precipitation, temperature, and NDVI of the four SM trend patterns exhibited significant increasing trends in 1982–2015, except for the D to D pattern with its precipitation increasing insignificantly (Fig. 6). The regional average SM significantly increased in the W to W pattern but reduced in the others. Among them, the trend of mean SM in W to D was not significant. Furthermore, the SM of D to D decreased faster than that of D to W by -0.1 × 10^{-3} m^3/ m^3 yr^{-1}. The above results indicate the rationality of the four SM trend patterns identified in the GVG areas.

In Fig. 7 and Table S1, SEM showed that the W to W pattern was greatly caused by vegetation greening in terms of the direct effects. The total effect of temperature exceeded that of vegetation on SM change, but its direct influence was not significant. Moreover, the rising temperature indirectly influenced SM change (soil wetting) by contributing to vegetation greening significantly. For the W to D pattern, NDVI, precipitation and temperature failed to explain the major trend of SM change ($R^2 = 0.29$), but relatively, the direct negative effect of temperature on SM was the strongest. The total effect of precipitation on SM change was the greatest but was not considered because NDVI had a non-significant direct effect on SM change. The increase in temperature played a major role in the D to W pattern in which the negative direct effect of temperature on SM change was crucial, but vegetation greening imposed a certain negative direct effect on SM change.
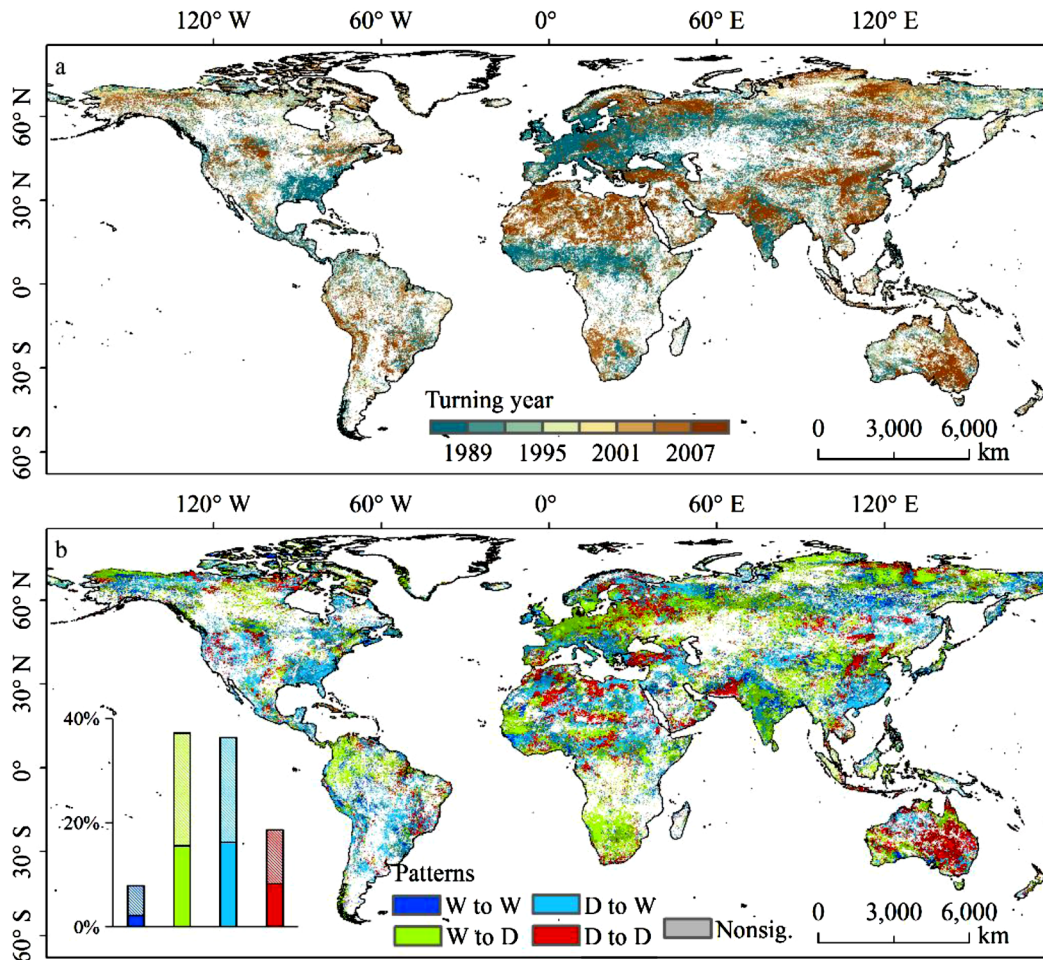
Fig. 4. Spatial distribution for turning years of NDVI mean values (a) and four patterns of SM trends (b). In Fig. 4b, the columnar stacked diagram shows the area proportion of each SM trend pattern, and the light and dark colors represent insignificant and significant proportions, respectively.
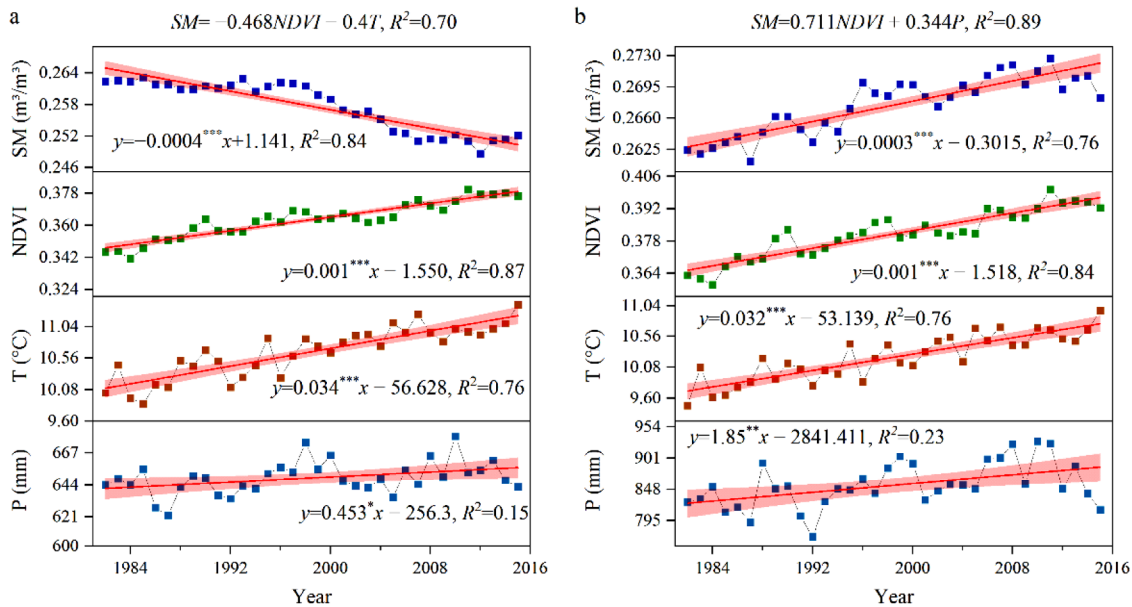
Fig. 5. Changes of area-averaged annual precipitation, temperature, NDVI, and SM in 1982–2015 for different scenarios. Fig. 5a and 5b are for global soil drying and vegetation greening areas as well as global soil wetting and vegetation greening areas respectively; P and T represent precipitation and temperature; ***, **, * are the significance levels at 0.001, 0.01, 0.05. The top of Fig. 5 are the stepwise regression equations of SM.
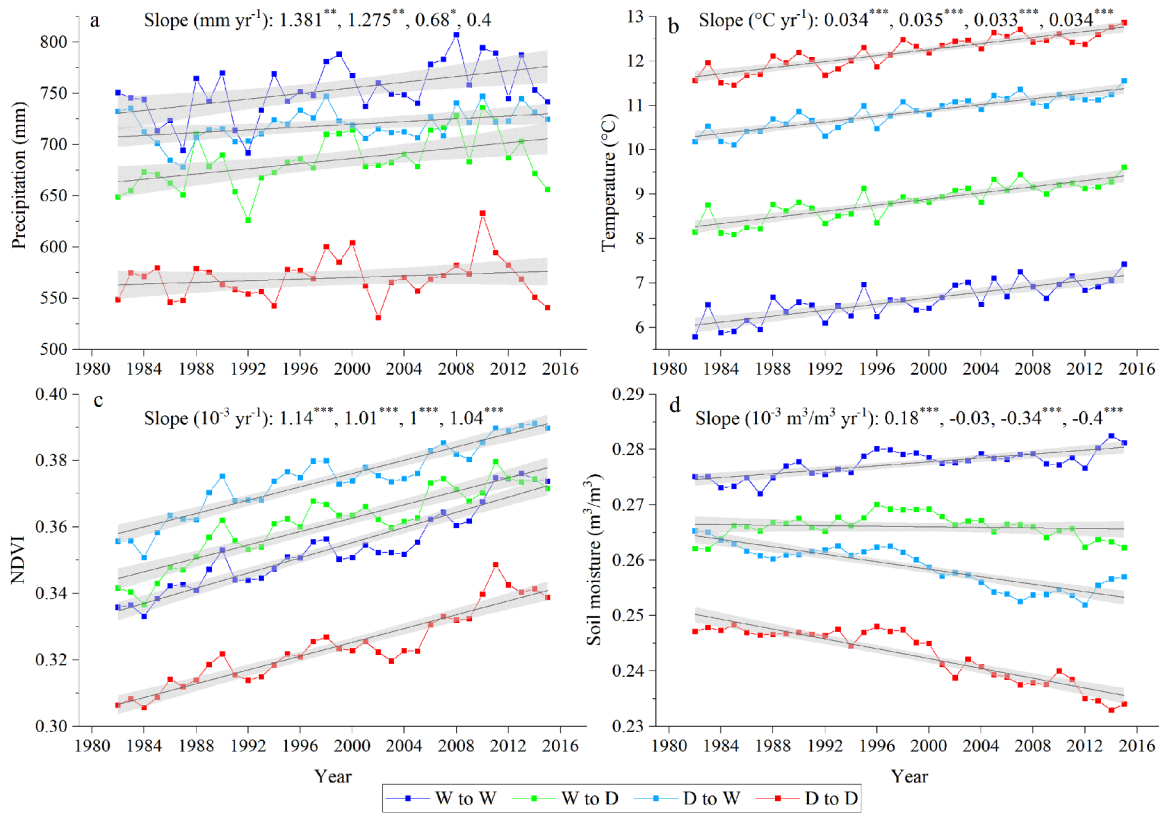
Fig. 6. Changes of regional average annual precipitation (a), temperature (b), NDVI (c), and SM (d) for four patterns of SM trend in 1982–2015. Slope is from the standardized coefficient of unary linear regression, the value order of which represents W to W, W to D, D to W, D to D patterns. ***, **, *are the significance levels at 0.001, 0.01, 0.05.
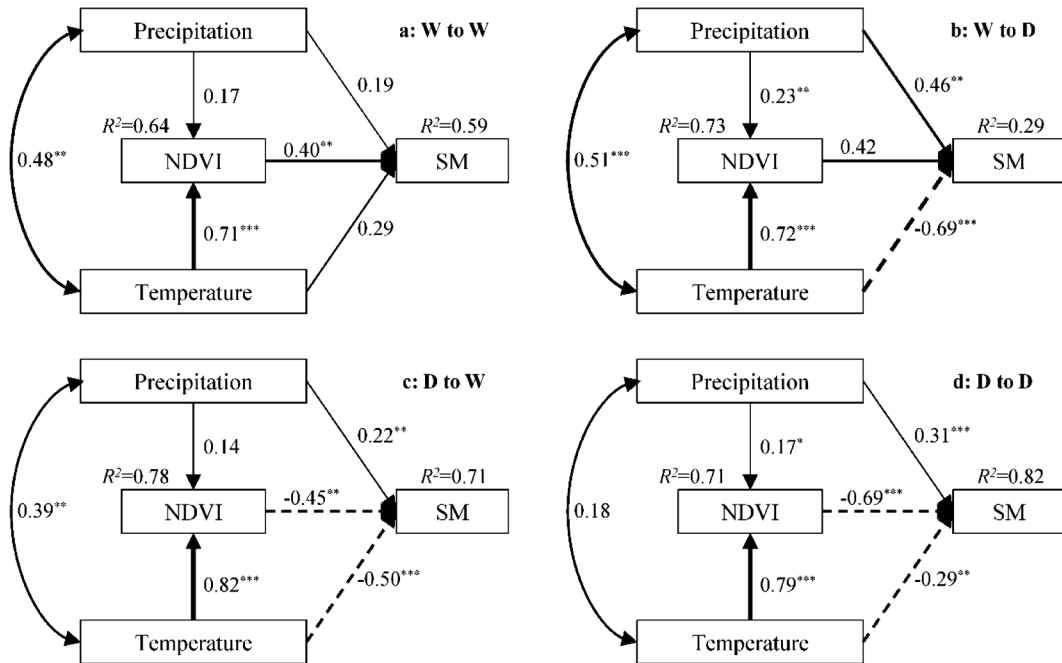
Fig. 7. Structural equation model results for the relationship among NDVI, precipitation, temperature and SM under four SM trend patterns. In Fig. 7, the box represents the observed variable; the one-way arrow indicates an effect relationship between the two variables, and the variable pointed by the arrow is affected by the other variable. The double-headed arrow denotes an association between the variables. The number near the single arrow or double-headed arrow is the normalized coefficient, and the solid (broken) line of the arrow indicates a positive (negative) relation, respectively, and the thicker the line, the stronger the relationship. ***, **, * are the significance levels at 0.01, 0.05, 0.1, respectively, and R^2 is the proportion of the variance explained.

Judging from the direct effect on the D to D pattern, vegetation greening played a leading part in the more drying trend of soil. Furthermore, the total effect of temperature on the enhancement of soil drying was the greatest; however, compared with its direct effect, the indirect effect of temperature on SM trend via promoting vegetation growth was more important. Besides, the coefficients between precipitation and temperature, representing the consistency of hydro-thermal change, indicated that increased vegetation tended to aggravate soil drying in areas with inconsistent water and heat changes. Therefore, in places where water and heat changes are conflicting, the growth of vegetation may be unsustainable, and forestry and conservation projects possibly cause soil drying problems.

In conclusion, under the background that the vegetation greening is mainly affected by the temperature rising, vegetation acts as a dominant direct role in the SM change of W to W and D to D patterns. Namely, the vegetation greening largely contributes to the intensification of the change trend for the area-averaged SM in nearly 26.45% of GVG areas (7.87% for W to W and 18.58% for D to D), which is consistent with our hypotheses. The significant negative effect of vegetation in the D to W pattern and the significant positive effect in W to D pattern seem to conflict with the hypotheses, which may mainly because the absolute linear results of SEM fail to directly express the reversal effect of vegetation on the trend of SM change. Nonetheless, compared with W to W and D to D patterns, the positive effect of vegetation in W to D pattern and the negative effect in D to W pattern are weaker, which also reflects the rationality of the four patterns and proves the action of increased vegetation in these patterns.

4. Discussion

4.1. Contributions of climate zones and land covers to global simultaneous greening and drying

The global vegetation change based on GIMMS-NDVI is similar to the results of previous studies in which the global vegetation-covered areas were dominated by the greening trend (Zhang et al., 2017). Seven greening clusters, including the sub-Saharan region, are generally consistent with the results of Chen et al. (2019) who adopted the leaf area index (LAI) data. However, SM in over 60% of the GVG areas experienced a decreasing trend in 1982–2015, the distribution of which

is also observed in previous research (Cai et al., 2009; Feng and Fu, 2013; Zhu et al., 2016). Under climate zones (Fig. 8a), it was found that the co-occurring vegetation greening and soil drying areas in the humid climate (i.e., Dry sub-humid and Humid) and arid climate (i.e., Hyper-arid, Arid and Semi-arid) account for 36.63% and 29.24% of the GVG areas respectively. However, Fig. 5 shows that obvious differences in climate and vegetation exist between D & G areas and W & G areas. The former climate was remarkably arider and vegetation greenness was slightly low. Based on the aridity index, the Mann-Whitney U test, a nonparametric test of two independent samples, proved that the climate in the D & W areas was significantly drier than that in W & G areas with the p-value below 0.001 (Figure 8b). Considering that vegetation itself is also affected by the climate at various spatial scales (Fridley and Wright, 2018; Myneni et al., 1997; Tietjen et al., 2017; Yang et al., 2019), it can be inferred that the effect of vegetation on SM is probably controlled by the climate. In addition, some studies proposed that under future global warming, "greener" and "drier" were projected to occur concurrently in the American West (Mankin et al., 2017), and surface SM was predicted to differ in change from total SM (Berg et al., 2017). Therefore, it is important to further predict or assess global vegetation changes and their impact on SM at various depths under elevated temperature.

Various vegetation types or land covers have different influence on precipitation and runoff, and then on the distribution of SM (Chen et al., 2007; D'Odorico et al., 2007; Yang et al., 2014). Fig. S4 reveals that 22.62% of GVG areas in 1982–2015 were from grasslands (10), thereby contrasting with the conclusion that the contribution to the observed global greening mainly came from croplands (Chen et al., 2019). It may be because Chen et al. (2019) used leaf area index (LAI) data closely related to the multiple cropping systems as the vegetation proxy. Through the spatial overlay analysis, it was found that the main co-occurring drying and greening land covers were grasslands (10), barren (16), savannas (9), open shrublands (7), woody savannas (8) and croplands (12), and they occupied 53.38% of the GVG areas, among which the grasslands were mostly distributed in the high-latitude area of northeast Canada, the southwest United States, Northern China, Mongolia and other areas (Figure 9). For each land cover type (Fig. S5), except for evergreen broadleaf forests (2), the soil drying areas in other land cover types exceeded 50% of their own vegetation greening areas; especially, SM in nearly 80% of the greening areas in deciduous
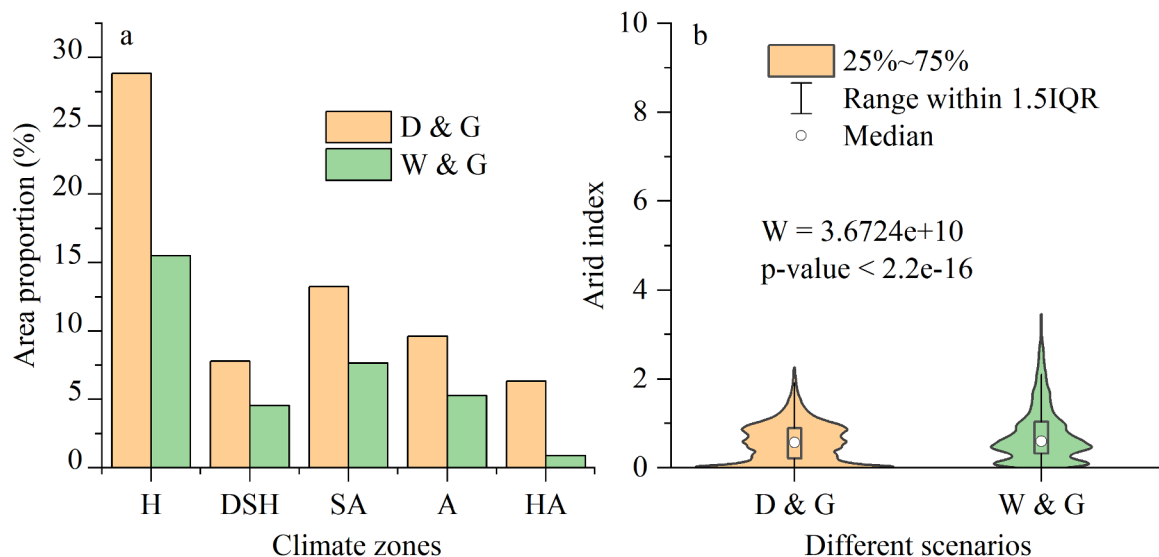
Fig. 8. Area proportion of co-occurring soil drying and vegetation greening areas as well as co-occurring soil wetting and vegetation greening areas in different climate zones (a) and the difference of aridity index between the two scenarios (b). In Fig. 8, D, W, and G represent soil drying, soil wetting, and vegetation greening respectively; in Fig. 8a, H, DSH, SA, A, HA represent Humid, Dry sub-humid, Semi-arid, Arid, Hyper-arid, respectively; in Fig. 8b, W and p-value are the results of the Mann-Whitney U test.
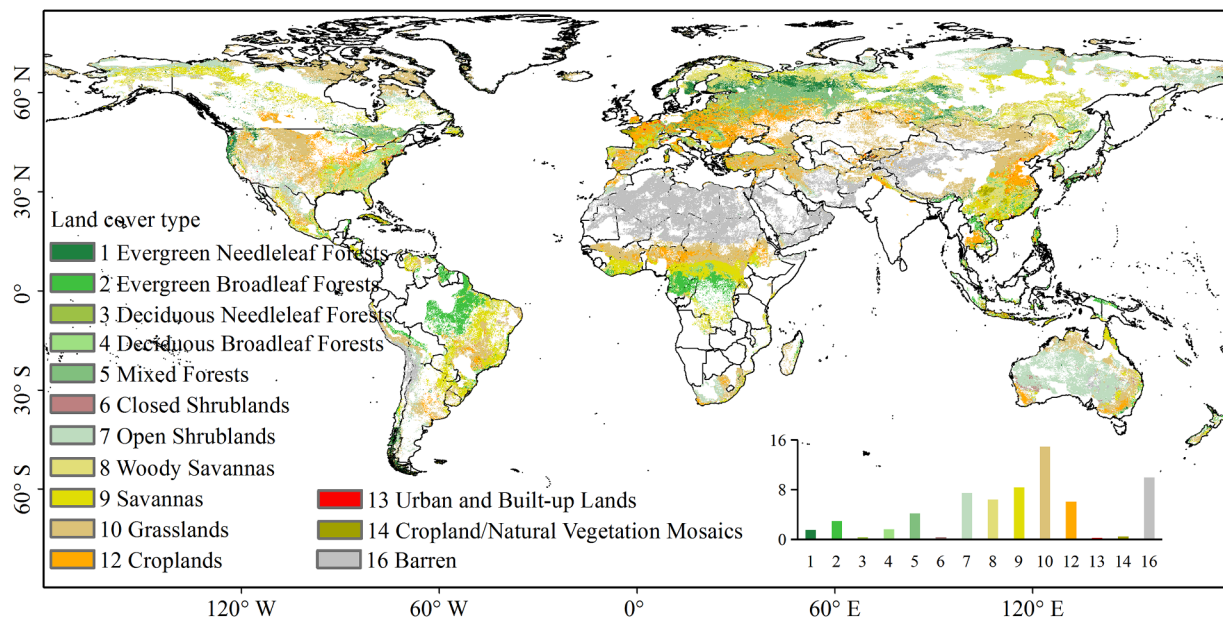
Fig. 9. Spatial distribution of land covers characterized by soil drying and vegetation greenness increasing. The inserted histogram shows the area proportion of each land cover with soil drying and vegetation greening in the GVG areas, unit: %.

broadleaf forests (4) reduced. Meanwhile, the averaged greening rates of vegetation in mixed forests (5), evergreen needleleaf forests (2), croplands (12), and cropland or natural vegetation mosaics (14) were higher than that of entire GVG areas, and the averaged rates of soil drying in the vegetation greening areas of barren (16), grasslands (10) and croplands (12) exceeded that of global greening and drying areas. Notably, the region-averaged vegetation greening and soil drying rates of croplands were higher than the average levels of the GVG areas.

4.2. Effects of vegetation greening on SM

4.2.1. Reliability of SM trend patterns

The study obtained the turning year when the mean value of NDVI increased significantly in GVG areas through the moving t-test and found that the global turning years obeyed the law that the year is generally later in the arider climate zones, and the median years of Humid, Dry sub-humid, Semi-arid, Arid and Hyper-arid areas were 1996, 1996, 1999, 2005 and 2006, respectively (Fig. S6). Most of the turning years in China were after 2000, and China has implemented the largest afforestation activities in the world since 1999 (Wang et al., 2013). Therefore, the determined turning year is relatively reliable.

This study applied SM from stations to preliminarily verify the four SM trend patterns identified by the turning year and observed that the NDVI matched with SM stations increased under the four patterns in 1982–2015, which coincided with the vegetation-greening characteristic of the study area. The Mann-Whitney U test revealed that the differences between the NDVI in P1 and P2 were remarkable, and the mean value in P1 was at least 0.9 less than that in P2. The W to W and W to D patterns were observed at their corresponding time series of SM from in-situ stations (Fig 10. a–b), though their trends of SM change were not significant in P1, and it may be the result of fewer stations in P1 compared with P2. The D to W pattern could not be confirmed in Fig. 10c, which is probably due to the large differences in the spatial distribution and number of stations in P1 and P2 (Fig. 1). The stations of the pattern were mainly distributed in low SM areas, such as the western United States, and increased sharply after 2005. For the D to D pattern, although SM increased rather than declined in P1, the in-situ observational SM of the D to D pattern performed the fastest declining trend in P2 among the four patterns. The above indicates that the

validation of four patterns requires more SM stations with even distribution and the longer observation length.

4.2.2. Function of vegetation greening in the D to D pattern

Previous research revealed that climate change, such as temperature rising (Deng et al., 2020b; Zhu et al., 2016), was the main cause of global soil drying (Cook et al., 2018). However, although vegetation has ecological services for soil and water conservation (Gu et al., 2013), increased vegetation can result in evaporation going up, consequently reducing SM (Feng et al., 2016; Yang et al., 2014). Considering that vegetation growth can absorb the groundwater (Koirala et al., 2017). Therefore, we followed Chen et al (2019) to divide the land cover types except barren (16) into four biome categories: Forests, Other woody vegetation (regarded as Shrublands in this study), Grasslands, and Croplands. According to the groundwater table depth (Fan et al., 2013), the median water table depths of Forests, Shrublands, Grasslands and Croplands in the study area are 11.53, 12.61, 16.25 and 11.32 m respectively, while their maximum root depths on the global scale are 7.0 ± 1.2, 5.1 ± 0.8, 2.6 ± 0.1 and 2.1 ± 0.2 m respectively (Canadell et al., 1996), indirectly suggesting that global vegetation mainly consumes SM.

After validation from SEM, we found that vegetation greening in some areas across the globe enhanced the trend of SM change. Particularly, in the D to D pattern, the direct effect of vegetation growth mainly contributed by temperature on SM was stronger than the direct or indirect effect of temperature. In Fig. 11, the median values of the turning years for the four SM trend patterns showed that vegetation greenness in half of the D to D areas increased significantly after 2005, and varying from other patterns mainly distributed in humid areas, the majority of the D to D areas were located in drylands (Semi-arid, Arid, and Hyper-arid areas). The previous study also revealed that the influence of vegetation on SM got stronger in semi-arid sand dunes (Wang et al., 2015). Moreover, D to D pattern was mainly observed in grasslands (10), barren (16), open shrublands (7), savannas (9), croplands (8), and other land covers (Table S2) and it was found that in water-restricted areas, the average root depths of herbaceous plants (annuals, perennial forbs, and grasses) is 0.28–1.04 m, and that of shrubs (dwarf-shrubs and shrubs) is 1.27–2.14 m (Costantini et al., 2016), which are shallower than the medians for groundwater table
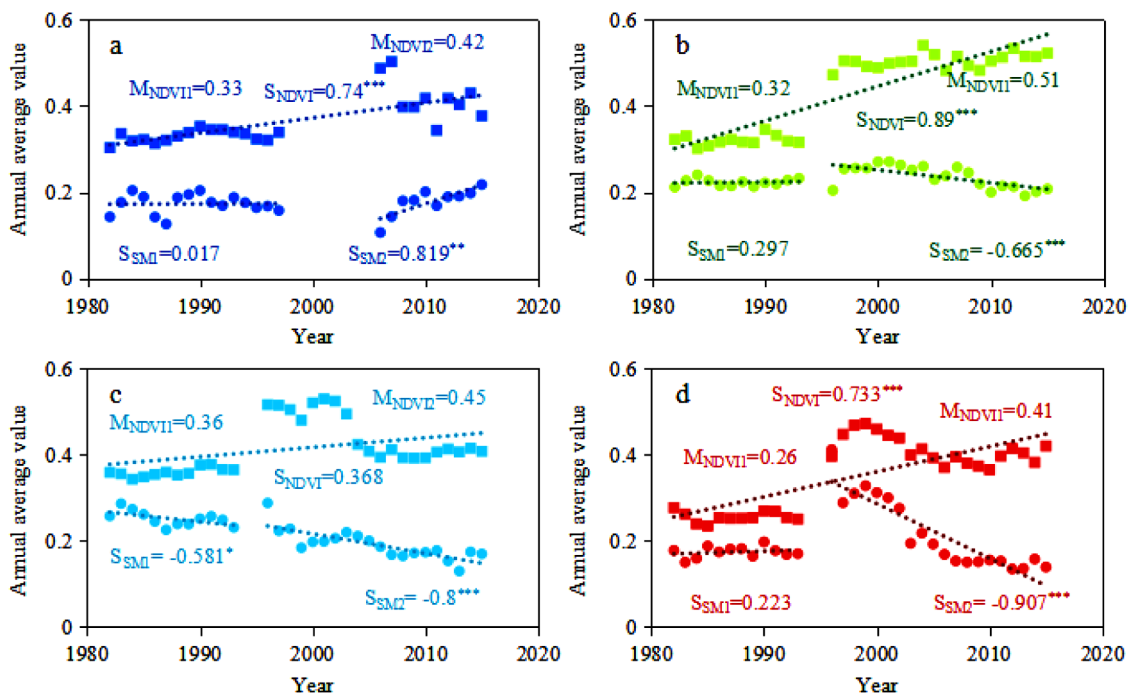
Fig. 10. SM from in-situ stations under the four patterns and their corresponding NDVI changes from 1982 to 2015. Fig. 10a–d are for the W to W, W to D, D to W, and D to D patterns, respectively, and the squares and dots represent NDVI and observational SM, respectively. M and S denote the mean value and the standardized line slope, respectively; the unit of mean SM is m^3/m^3. NDVI1 and SM1 represent the NDVI and SM in the hypothetical reference period (P1) and NDVI2 and SM2 are NDVI and SM in the assumed period when the average NDVI increased remarkably (P2); ***, **, * are the significance levels at 0.001, 0.01, 0.05, respectively.

depths of grasslands, barren, and open shrublands in D to D areas and GVG areas (Fig. 11c), indicating that SM is the major water source of vegetation growth in the D to D pattern. In summary, it can be inferred that temperature (in this study), CO_2 concentration (Morgan et al., 2011), human activities (Fensholt et al., 2012), etc. promote the initial increase of vegetation in D to D areas. However, with the water demand for vegetation greening augmenting, plenty of SM in D to D areas is converted to biological water and then consumed by vegetation
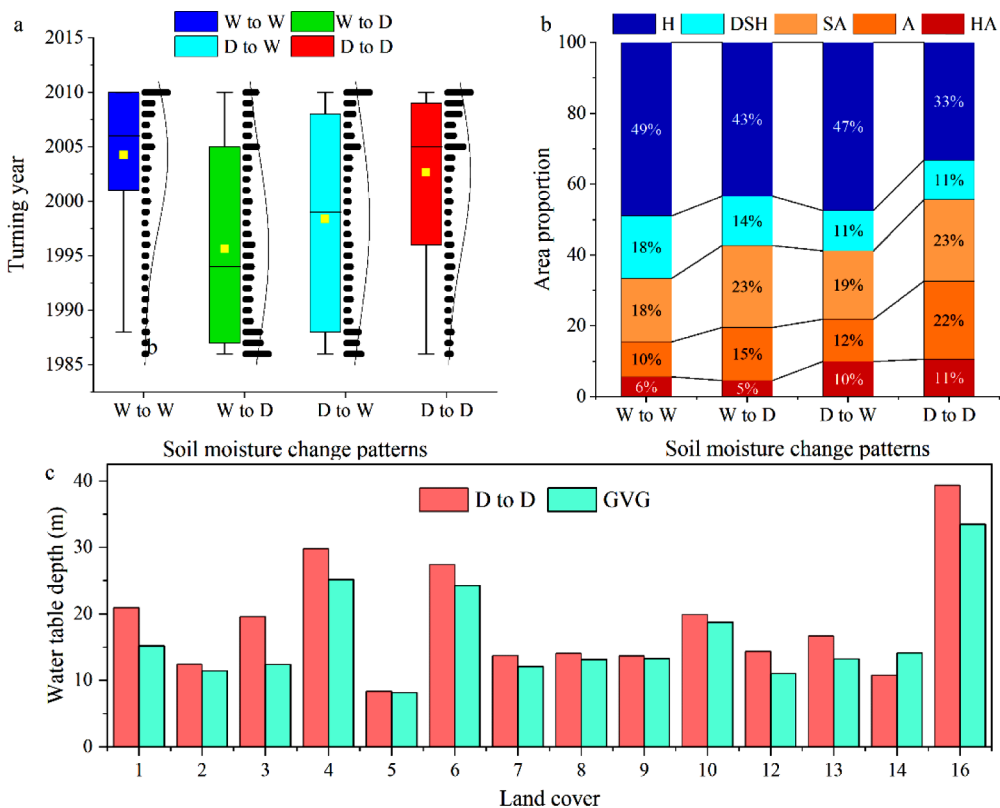
Fig. 11. Box plot (a) of the turning years and the area proportion stacked plot (b) of each climatic zone in four SM trend patterns and the water table depths (c) of land covers in D to D pattern and GVG areas. In Fig. 11b, H, DSH, SA, A, HA represent Humid, Dry sub-humid, Semi-arid, Arid, Hyper-arid, respectively. See Fig. 9 for the specific types represented by land cover code.

transpiration and the rising temperature also enhances evaporation (Naumann et al., 2018), then generating the sharp decrease of SM in the drylands where the precipitation is less than evapotranspiration (Tietjen et al., 2017). Worse, a soil drying layer is formed and difficult to recover, such as the Loess Plateau in China (Yang et al., 2014), and vegetation degenerates and dies due to lack of water, which is not conducive to long-term global greening and sustainable ecosystem development in Semi-arid, Arid and Hyper-arid areas (Xia and Shao, 2008). Overall, in the averaged global root profile, about 75% of roots were distributed in the top 40 cm of soil (Jackson et al., 1996), and SM at the soil depth of 5 cm captured the information in 0-60 cm SM and was suitable for the drought monitoring applications (Qiu et al., 2014). Therefore, the feedback, especially the soil drought status, of 0-7 cm SM on vegetation greening can provide a certain reference significance for the study of vegetation ecohydrology. However, the effects of multiple vegetation types on SM change vary at different soil depths via physical and ecological processes (Fan et al., 2017), and it is necessary for the more comprehensive understanding of the eco-hydrological function of vegetation to compare the responses of surface and deep SM to vegetation growth based on adequate data from stations.

5. Conclusions

Based on high-quality data from remote sensing, reanalysis, and ground stations, we used Theil-Sen trend analysis, MK test, and the structural equation model to verify whether vegetation greening exerts a positive or negative effect on SM. The conclusions are the following:

1) From 1982 to 2015, SM in over three-fifths (33.57%, Sig.) of GVG areas decreased, mainly located in the southeast of the United States, Africa north of the equator, the south of China and other humid areas (36.63% of GVG areas), and the central of North America, the north of China, the inland of Australia, the Saharan in Africa and other drylands (29.24% of GVG areas).

2) The main land cover contributing to co-occurring soil drying and vegetation greening areas came from grasslands. The vegetation greening rate and SM decreasing rate of croplands were faster than the average levels of GVG areas.

3) Vegetation increase exerted a positive effect on the average SM in the global greening and wetting areas but a negative effect in global greening and drying areas, and ,remarkably, climate of the latter was arider, with their difference of the average annual precipitation among 133.62–272.42 mm.

4) SM trends in 55.77% of the GVG areas were directed toward drying after the statistically significant increase in the average of vegetation greenness; the trend of SM change from drying to more drying was mainly distributed in Semi-arid, Arid, and Hyper-arid areas.

5) Structural equation model showed that the change trend of average SM in 26.45% of the GVG areas (7.87% and 18.58% for the W to W and D to D patterns, respectively) was strengthened by vegetation greening. Among them, in the D to D pattern, the direct effect of increased vegetation mainly promoted by temperature rising on the intensification of soil drying exceeded the direct or indirect effect of temperature on SM.

6) Preliminary verification from the SM of limited stations indicated that the W to W and W to D patterns were reliable. Simultaneously, based on the depths of groundwater table and plant root, the water consumed by vegetation greening in D to D areas fundamentally came from SM. Therefore, in these areas, soil-water balance should be considered in vegetation management.

In the future, the contributions of soil evaporation and vegetation transpiration to soil drying can be explored to further validate the findings in the study. Meanwhile, the hydrological effects of vegetation increase are complex and nonlinear. Therefore, it requires nonlinear hydrological models as well as more and longer observation data to simulate and evaluate the effects of vegetation change on SM.

Declaration of Competing Interest

The authors declare that they have no known competing financial interests or personal relationships that could have appeared to influence the work reported in this paper.

Supplementary materials

Supplementary material associated with this article can be found, in the online version, at doi:10.1016/j.agrformet.2020.108103.

References

Adair, E.C., Reich, P.B., Trost, J.J., Hobbie, S.E., 2011. Elevated CO₂ stimulates grassland soil respiration by increasing carbon inputs rather than by enhancing soil moisture. Global Change Biol. 17 (12), 3546–3563.

Albergel, C., De Rosnay, P., Balsamo, G., Isaksen, L., Munoz-Sabater, J., 2012. Soil Moisture Analyses at ECMWF: Evaluation Using Global Ground-Based In Situ Observations. J. Hydrometeorol. 13 (5), 1442–1460.

Ali, S., Dan, L., Fu, C.B., Khan, F., 2015. Twenty first century climatic and hydrological changes over Upper Indus Basin of Himalayan region of Pakistan. Environ. Res. Lett. 10 (1), 014007.

Berg, A., Sheffield, J., Milly, P.C.D., 2017. Divergent surface and total soil moisture projections under global warming. Geophys. Res. Lett. 44 (1), 236–244.

Brandt, M., Rasmussen, K., Peñuelas, J., et al., 2017. Human population growth offsets climate-driven increase in woody vegetation in sub-Saharan Africa. Nat. Ecol. & Evol. 1 (4).

Cai, W.J., Cowan, T., Briggs, P., Raupach, M., 2009. Rising temperature depletes soil moisture and exacerbates severe drought conditions across southeast Australia. Geophys. Res. Lett. 36.

Canadell, J., Jackson, R.B., Ehleringer, J.R., et al., 1996. Maximum rooting depth of vegetation types at the global scale. Oecologia 108 (4), 583–595.

Chen, C., Park, T., Wang, X.H., et al., 2019. China and India lead in greening of the world through land-use management. Nat. Sustainability 2 (2), 122–129.

Chen, L.D., Huang, Z.L., Gong, J., Fu, B.J., Huang, Y.L., 2007. The effect of land cover/vegetation on soil water dynamic in the hilly area of the loess plateau. China. Catena 70 (2), 200–208.

Cook, B.I., Mankin, J.S., Anchukaitis, K.J., 2018. Climate Change and Drought: From Past to Future. Curr. Clim. Change Rep. 4 (2), 164–179.

Costantini, E.A.C., Branquinho, C., Nunes, A., et al., 2016. Soil indicators to assess the effectiveness of restoration strategies in dryland ecosystems. Solid Earth 7 (2), 397–414.

Deng, Y.H., Wang, S.J., Bai, X.Y., et al., 2020a. Comparison of soil moisture products from microwave remote sensing, land model, and reanalysis using global ground observations. Hydrol. Process. 34 (3), 836–851.

Deng, Y.H., Wang, S.J., Bai, X.Y., et al., 2019. Characteristics of soil moisture storage from 1979 to 2017 in the karst area of China. Geocarto Int. 24, 1–15.

Deng, Y.H., Wang, S.J., Bai, X.Y., et al., 2020b. Variation trend of global soil moisture and its cause analysis. Ecol. Indic. 110, 105939.

D'odorico, P., Caylor, K., Okin, G.S., Scanlon, T.M., 2007. On soil moisture-vegetation feedbacks and their possible effects on the dynamics of dryland ecosystems. J. Geophys. Res.-Biogeo. 112 (G4).

De Jong, R., De Bruin, S., De Wit, A., Schaepman, M.E., Dent, D.L., 2011. Analysis of monotonic greening and browning trends from global NDVI time-series. Remote Sens. Environ. 115 (2), 692–702.

D'odorico, P., Laio, F., Porporato, A., et al., 2010. Ecohydrology of Terrestrial Ecosystems.

Bioscience 60 (11).

Dorigo, W.A., Wagner, W., Hohensinn, R., et al., 2011. The International Soil Moisture Network: a data hosting facility for global in situ soil moisture measurements. Hydrol. Earth Syst. Sc. 15 (5), 1675–1698.

Fan, Y., Li, H., Miguez-Macho, G., 2013. Global Patterns of Groundwater Table Depth. Science 339 (6122), 940–943.

Fan, Y., Miguez-Macho, G., Jobbagy, E.G., Jackson, R.B., Otero-Casal, C., 2017. Hydrologic regulation of plant rooting depth. P. Natl. Acad. Sci. USA 114 (40), 10572–10577.

Fauchald, P., Park, T., Tommervik, H., Myneni, R., Hausner, V.H., 2017. Arctic greening from warming promotes declines in caribou populations. Sci. Adv. 3 (4).

Feng, S., Fu, Q., 2013. Expansion of global drylands under a warming climate. Atmos. Chem. Phys. 13 (19), 10081–10094.

Feng, T.J., Wei, W., Chen, L.D., Keesstra, S.D., Yang, Y., 2018. Effects of land preparation and plantings of vegetation on soil moisture in a hilly loess catchment in China. Land Degrad. & Dev. 29 (5), 1427–1441.

Feng, X.M., Fu, B.J., Piao, S.L., et al., 2016. Revegetation in China's Loess Plateau is approaching sustainable water resource limits. Nat. Clim. Change 6 (11), 1019–1022.

Fensholt, R., Langanke, T., Rasmussen, K., et al., 2012. Greenness in semi-arid areas across the globe 1981-2007—an Earth Observing Satellite based analysis of trends and drivers. Remote Sens. Environ. 121, 144–158.

Fridley, J.D., Wright, J.P., 2018. Temperature accelerates the rate fields become forests. P. Natl. Acad. Sci. USA 115 (18), 4702–4706.

Friedl, M.A, McIver, D.K., Hodges, J.C., et al., 2002. Global land cover mapping from MODIS: algorithms and early results. Remote Sens. Environ. 83 (1–2), 287–302.

Gu, Z.J., Wu, X.X., Feng, Z., et al., 2013. Estimating the effect of Pinus massoniana Lamb plots on soil and water conservation during rainfall, events using vegetation fractional coverage. Catena 109, 225–233.

Huang, K., Xia, J.Y., Wang, Y.P., et al., 2018. Enhanced peak growth of global vegetation and its key mechanisms. Nat. Ecol. & Evol. 2 (12), 1897–1905.

Jackson, R.B., Canadell, J., Ehleringer, J.R., et al., 1996. A global analysis of root distributions for terrestrial biomes. Oecologia 108 (3), 389–411.

Jöreskog, K.G., 1970. A general method for estimating linear structural equation systems. 1970(2):1-41.

Jost, G., Schume, H., Hager, H., Markart, G., Kohl, B., 2012. A hillslope scale comparison of tree species influence on soil moisture dynamics and runoff processes during intense rainfall. J. Hydro. 420, 112–124.

Koirala, S., Jung, M., Reichstein, M., et al., 2017. Global distribution of groundwater-vegetation spatial covariation. Geophys. Res. Lett. 44 (9), 4134–4142.

Li, X., Yang, D.W., Zheng, C.M., et al., 2017. Ecohydrology. In: Leng, S., Gao, X., Pei, T., Zhang, G. (Eds.), Geographical Sciences during 1986-2015: From the Classics to the Frontiers. Springer Geography, pp. 407–417.

Li, Y., Piao, S.L., Li, L.Z.X., et al., 2018. Divergent hydrological response to large-scale afforestation and vegetation greening in China. Sci. Adv. 4 (5).

Liu, J.G., Yang, H., Gosling, S.N., et al., 2017. Water scarcity assessments in the past, present, and future. Earths Future 5 (6), 545–559.

Lu, X.F., Wang, L.X., Mccabe, M.F., 2016. Elevated CO_2 as a driver of global dryland greening. Sci. Rep. 6.

Mankin, J.S., Seager, R., Smerdon, J.E., et al., 2018. Blue water trade-offs with vegetation in a CO_2-enriched climate. Geophys. Res. Lett. 45 (7), 3115–3125.

Mankin, J.S., Smerdon, J.E., Cook, B.I., Williams, A.P., Seager, R., 2017. The Curious Case of Projected Twenty-First-Century Drying but Greening in the American West. J. Climate 30 (21), 8689–8710.

Morgan, J.A., LeCain, D.R., Pendall, E., et al., 2011. C-4 grasses prosper as carbon dioxide eliminates desiccation in warmed semi-arid grassland. Nature 476 (7359), 202–205.

Myneni, R.B., Keeling, C.D., Tucker, C.J., Asrar, G., Nemani, R.R., 1997. Increased plant growth in the northern high latitudes from 1981 to 1991. Nature 386 (6626), 698–702.

Naumann, G., Alfieri, L., Wyser, K., et al., 2018. Global Changes in Drought Conditions Under Different Levels of Warming. Geophys. Res. Lett. 45 (7), 3285–3296.

Oh, H., Ha, K.J., 2016. Prediction of dominant intraseasonal modes in the East Asian-western North Pacific summer monsoon. Clim. Dynam. 47 (7-8), 2025–2037.

Porporato, A., D'odorico, P., Laio, F., Ridolfi, L., Rodriguez-Iturbe, I., 2002. Ecohydrology of water-controlled ecosystems. Adv. Water Resour. 25 (8-12), 1335–1348.

Qiu, J., Crow, W.T., Nearing, G.S., Mo, X., Liu, S., 2014. The impact of vertical measurement depth on the information content of soil moisture times series data. Geophys. Res. Lett. 41 (14), 4997–5004.

Rodriguez-Iturbe, I., 2000. Ecohydrology: A hydrologic perspective of climate-soil-vegetation dynamics. Water Resour. Res. 36 (1), 3–9.

Shi, Z., Xu, X., Souza, L., et al., 2016. Dual mechanisms regulate ecosystem stability under decade-long warming and hay harvest. Nat. Commun. 7.

Silva, L.C.R., Sun, G., Zhu-Barker, X., et al., 2016. Tree growth acceleration and expansion of alpine forests: The synergistic effect of atmospheric and edaphic change. Sci. Adv. 2 (8).

Stocker, B.D., Zscheischler, J., Keenan, T.F., et al., 2019. Drought impacts on terrestrial primary production underestimated by satellite monitoring. Nat. Geosci. 12 (4), 264–270.

Stothoff, S.A., Or, D., Groeneveld, D.P., Jones, S.B., 1999. The effect of vegetation on infiltration in shallow soils underlain by fissured bedrock. J. Hydro. 218 (3-4), 169–190.

Sun, G., Zhou, G.Y., Zhang, Z.Q., et al., 2006. Potential water yield reduction due to forestation across China. J. Hydro. 328 (3–4), 548–558.

Tietjen, B., Schlaepfer, D.R., Bradford, J.B., et al., 2017. Climate change-induced vegetation shifts lead to more ecological droughts despite projected rainfall increases in many global temperate drylands. Global Change Biol 23 (7), 2743–2754.

Tong, X.W., Brandt, M., Yue, Y.M., et al., 2018. Increased vegetation growth and carbon stock in China karst via ecological engineering. Nat. Sustainability 1 (1), 44–50.

Veldkamp, T.I.E., Wada, Y., Aerts, J.C.J.H., Ward, P.J., 2016. Towards a global water scarcity risk assessment framework: incorporation of probability distributions and hydro-climatic variability. Environ. Res. Lett. 11 (2).

Wang, J.Y., Liu, Y.S., Liu, Z.G., 2013. Spatio-Temporal Patterns of Cropland Conversion in Response to the "Grain for Green Project" in China's Loess Hilly Region of Yanchuan County. Remote Sens 5 (11), 5642–5661.

Wang, T.J., Wedin, D.A., Franz, T.E., Hiller, J., 2015. Effect of vegetation on the temporal stability of soil moisture in grass-stabilized semi-arid sand dunes. J. Hydro. 521, 447–459.

Weterings, R., Umponstira, C., Buckley, H.L., 2018. Landscape variation influences trophic cascades in dengue vector food webs. Sci. Adv. 4 (2).

Xia, Y.Q., Shao, M.A., 2008. Soil water carrying capacity for vegetation: A hydrologic and biogeochemical process model solution. Ecol. Model. 214 (2-4), 112–124.

Yang, L., Wei, W., Chen, L.D., Chen, W.L., Wang, J.L., 2014. Response of temporal variation of soil moisture to vegetation restoration in semi-arid Loess Plateau. China. Catena 115, 123–133.

Yang, Y.J., Wang, S.J., Bai, X.Y., et al., 2019. Factors Affecting Long-Term Trends in Global NDVI. Forests 10 (5).

Zeng, Z.Z., Peng, L.Q., Piao, S.L., 2018. Response of terrestrial evapotranspiration to Earth's greening. Curr. Opin. Env. Sust. 33, 9–25.

Zhang, C.Q., Zhang, B., Li, W.H., Liu, M.C., 2014. Response of streamflow to climate change and human activity in Xitiaoxi river basin in China. Hydrol. Process. 28 (1), 43–50.

Zhang, X.Z., Wun, X.Y., He, J.H., 2004. Vertical character of soil moisture in china. Acta Meteorol. Sin. 62 (1), 51–61.

Zhang, Y.L., Song, C.H., Band, L.E., Sun, G., Li, J.X., 2017. Reanalysis of global terrestrial vegetation trends from MODIS products: Browning or greening? Remote Sens. Environ 191, 145–155.

Zhao, L., Dai, A.G., Dong, B., 2018. Changes in global vegetation activity and its driving factors during 1982-2013. Agric. For. Meteorol. 249, 198–209.

Zhu, Z.C., Piao, S.L., Myneni, R.B., et al., 2016. Greening of the Earth and its drivers. Nat. Clim. Change 6 (8), 791–795.